

## Article

# Rice Husk as Raw Material in Synthesis of NaA (LTA) Zeolite

Daniela Novembre <sup>1</sup>, Domingo Gimeno <sup>2,\*</sup>, Lucia Marinangeli <sup>3</sup>, Anna Chiara Tangari <sup>3</sup>,  
Gianluigi Rosatelli <sup>3</sup>, Michele Ciulla <sup>4</sup> and Pietro di Profio <sup>4</sup>

<sup>1</sup> Dipartimento di Ingegneria e Geologia, Università degli Studi "G. D'Annunzio", Via dei Vestini 30, 66013 Chieti, Italy; daniela.novembre@unich.it

<sup>2</sup> Department Mineralogia, Petrologia i Geologia Aplicada, Universitat de Barcelona, 08028 Barcelona, Spain

<sup>3</sup> Dipartimento di Scienze Psicologiche, della Salute e del Territorio, Università degli Studi "G. D'Annunzio", Via dei Vestini 30, 66013 Chieti, Italy; lucia.marinangeli@unich.it (L.M.); a.tangari@unich.it (A.C.T.); g.rosatelli@unich.it (G.R.)

<sup>4</sup> Department of Pharmacy, University of Chieti-Pescara "G. d'Annunzio", Via dei Vestini, 6100 Chieti, Italy; michele.ciulla@unich.it (M.C.); pietero.diprofio@unich.it (P.d.P.)

\* Correspondence: d.gimeno.torrente@gmail.com or domingo.gimeno@ub.edu; Tel.: +34-934021404

**Abstract:** The present work deals with the hydrothermal synthesis of a Na-A (LTA) zeolite using rice husk as a starting material. The focus was on defining the most favorable conditions for the synthesis of zeolite Na-A from rice husk in order to economize on both energy (i.e., synthesis temperatures) and reaction time and to enlarge the field of the pure and isolated synthesized phase. Four sets of experiments were carried out at environmental pressure temperatures varying from 40 °C to 85 °C with a SiO<sub>2</sub>/Al<sub>2</sub>O<sub>3</sub> ratio from 1.75 to 3.5. Optimal conditions for crystallization of the Na-A zeolite from rice husk were reached at 60 °C with a SiO<sub>2</sub>/Al<sub>2</sub>O<sub>3</sub> ratio of 1.75. Sixty degrees Celsius represents the minimum known temperature used for the synthesis of NaA zeolite from rice husk. The products of synthesis were characterized by X-ray diffraction, scanning electron microscopy, infrared and Raman spectroscopy. The purity of the synthesized zeolite is verified here for the first time through quantitative phase analysis using the combined Rietveld and reference intensity ratio methods.

**Keywords:** zeolites; rice husk ash; X-ray diffraction; synthesis; NaA LTA Zeolite



**Citation:** Novembre, D.; Gimeno, D.; Marinangeli, L.; Tangari, A.C.; Rosatelli, G.; Ciulla, M.; di Profio, P. Rice Husk as Raw Material in Synthesis of NaA (LTA) Zeolite. *Molecules* **2024**, *29*, 4396. <https://doi.org/10.3390/molecules29184396>

Academic Editor: Jerzy Datka

Received: 7 August 2024

Revised: 9 September 2024

Accepted: 12 September 2024

Published: 16 September 2024



**Copyright:** © 2024 by the authors. Licensee MDPI, Basel, Switzerland. This article is an open access article distributed under the terms and conditions of the Creative Commons Attribution (CC BY) license (<https://creativecommons.org/licenses/by/4.0/>).

## 1. Introduction

Rice husk (RH) is an agricultural waste available in rice-producing countries. The potential global RH production is estimated at 21 million tons per year [1]. Generally, much of the husk is burnt or dumped as waste; sometimes, it is converted into end products such as feedstock [2] and adsorbents [3] or is used as a resource of combustion for electricity generation in those countries dependent on imported oil for their energy needs [4]. In many cases, it is burned openly, causing environmental and health problems, especially in poor and developing countries [5]. In some cases, RH is burned in the boiler of various industries to produce RH ash (RHA) which contains 96–99 wt% of amorphous SiO<sub>2</sub> [6]. RHA can represent a cheap alternative for silica for many industrial uses [7], being a highly reactive reactant for many chemical processes. Barthey et al. [8] used RH silica as a raw material for producing solar-grade silicon (Si-GS) and Johar et al. [9] produced mullite for the ceramic industry starting from RH. RH was also used as an alternative source of silica to synthesize zeolites [10–19]. Zeolites are crystalline aluminosilicates characterized by an open three-dimensional framework structure built of SiO<sub>4</sub> and AlO<sub>4</sub> tetrahedra linked by sharing oxygens to form regular intracrystalline cavities and channels of atomic dimensions [20]. The ion exchange and the selective adsorption properties of zeolites are at the base of several industrial uses. Some of them deal with radioactive wastewater treatment, sewage effluent treatment, agricultural-wastewater treatment [21], etc.

Among low-silica sodium zeolites, the NaA zeolite deserves attention. This zeolite is characterized by two cage types in its lattice: the β-cage (sodalite cage) and α-cage [22].

Eight sodalite cages are connected through double four-membered rings to create a large  $\alpha$ -supercage in the middle of eight-membered rings [23]. The Si/Al ratio of 1 confers to the structure a high cation exchange capacity. The most common application is in the field of water detergency. NaA is in fact largely used by the detergent industry in countries with restrictive environmental regulations; it substitutes Na tripoliphosphate (NTP), one of the main pollutants responsible for the eutrophication of superficial waters [24]. There are also studies on the absorption of methane [25], carbon dioxide [26], ethylene and propylene [27] by Zeolite NaA. It is also used in the dehydration of ethanol [28] and as an antimicrobial material when exchanged with silver ions [29].

Zeolites are generally synthesized from solutions of sodium silicate and sodium aluminate [30] or from natural materials. The nature of the raw materials strongly influences the purity and quality of the synthesized zeolites [31]. Zeolite synthesis has been performed using different kinds of natural precursors such as kaolinite [32–35]; bentonite [36,37]; smectite [38]; mordenite [39]; halloysite [40,41]; tripolaceous and volcanic rocks [21,42] and industrial waste materials [43–45]. Among waste materials, RH was also used in the synthesis of low-silica sodium zeolites [6,46–55].

Nur et al. [46] reported the synthesis of NaA zeolites starting from RH; crystallization is performed at 100 °C in 5 h but there is a tendency for formation of amorphous phases in the NaA zeolite. Petkowicz et al. [6] and Bhavornthanayod et al. [4] reported the synthesis of a zeolite A membrane from RHA at 100 °C in 4 h. Yusof et al. [47] established the conversion of RH in a NaA-type zeolite at 100 °C in 6 h. Azizi et al. [48] used microwave-assisted and hydrothermal conventional heating to synthesize a NaA zeolite from RH; after 2 h of microwave heating, the mixture is conventionally hydrothermally treated at 180 °C for 16 h. These authors stated that the combined hydrothermal–microwave technique improves the kinetics in the synthesis of zeolites; however, this is highly questionable given the previous works cited before [6,46,47]. Moreover, the X-ray diffractometric spectrum of NaA lacks the characteristic peaks at  $7.10^\circ 2\theta$  typical of this zeolite [56]. In 2011, Tan et al. [49] reported the synthesis of NaA from RHA at 100 °C in 5 h. More recently, nanocrystals of NaA ranging from 50 to 120 nm were synthesized by Ghasemi and Younesi [50] at room temperature with 3 days aging and without any organic additives. The same authors reported the synthesis of nanocrystals of NaA, ranging from 40 to 120 nm, obtained at 40 °C with 18 h aging [51]. Tepamat et al. [52] synthesized Na-A zeolites from rice husk at 100 °C in 8 h. Ahmedzeki et al. [53] reported the synthesis of NaA zeolites starting from aluminum cans and rice husk; synthesis was performed at 100 °C in a day. Wang et al. [54] synthesized NaA zeolites by the hydrothermal method with seed technology at a temperature of 100 °C for 12 h, while Madhu et al. [55] obtained NaA zeolites from rice husk at 100 °C in 8 h.

As can be seen, apart from the works of Ghasemi and Younesi [50,51] regarding the synthesis of nanosized crystals of NaA zeolites, all the past literature indicates 100 °C as the best lowest temperature at which a zeolite crystallizes.

Considering the previous literature, this work aims to investigate the best condition for the synthesis of NaA zeolites starting from RH. In this paper, we present the results of research carried out to define the most favorable conditions to economize both energy (i.e., synthesis and calcination temperatures) and reaction time. In particular, the work aims on the one hand to lower the rice calcination temperatures below 600 °C and on the other to reduce the synthesis temperatures below 100 °C. The influence of the  $\text{SiO}_2/\text{Al}_2\text{O}_3$  ratios is also investigated.

In recent decades, there has been a renewed interest in NaA zeolites and there has been an increase in the number of scientific publications on the synthesis and applications of this zeolite, as highlighted by Collins et al. [23]. Although the bibliography attests to a wide development of innovative methodologies aimed at the synthesis of this mineral starting from rice husk, it must be said that no industrial transfer followed any protocol. Collins et al. [23] find reasons for this in terms of the manufacturing cost and development of new markets. In our opinion, one of the reasons for this may probably be the lack of quantitative characterizations on the purity of the synthesized products; as is known, one of the essential

requirements of the industry is at least 90% purity of the products obtained. Regarding this, none has quantitatively characterized the product of the synthesis yet. The identification of the zeolite peaks in the diffraction spectrum is not sufficient for defining the experimental protocol as successful. What does matter is the estimation of the amorphous phase and/or unreacted reagents in the final product. This is of crucial importance for useful minerals such as zeolites whose usage strongly depends on the purity of powders, which drives their efficacy in technological applications. Alongside a complete spectrum of characterization of the synthesized powders, a quantitative analysis of them will allow us to determine the contribution of the amorphous component and/or other unreacted phases.

This will help to accurately define the purity of the synthesis powders and will pave the way for an industrial transfer of the synthesis protocol.

## 2. Results and Discussion

Figure 1a reports the X-ray Powder Diffraction (XRPD) spectrum of RHA, revealing an amorphous character, as is evident from the absence of peaks and the presence of the hump around the  $20^\circ$  of 2 theta.

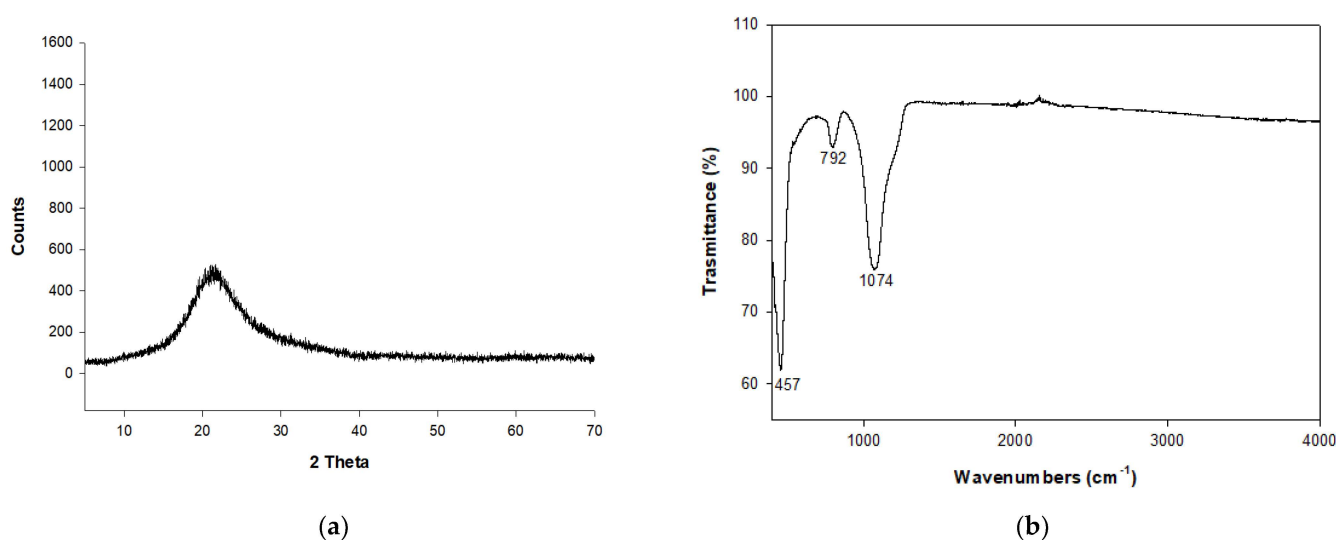


**Figure 1.** (a) XRPD pattern of RHA. (b) IR analysis on RHA.

Figure 1b shows the results of infrared (IR) analysis on RHA. There is a strong band at  $1074\text{ cm}^{-1}$ , a medium band at  $792\text{ cm}^{-1}$  and another strong and narrow band at  $457\text{ cm}^{-1}$ . The vibration at  $1074\text{ cm}^{-1}$  can be assigned to the asymmetric stretching vibrations of tetrahedral  $\text{SiO}_4$ , while the peak at  $792\text{ cm}^{-1}$  is related to the symmetric stretching of  $\text{SiO}_4$  tetrahedra. The signal at  $457\text{ cm}^{-1}$  is associated with the Si-O bending mode. Data are coherent with findings from Petkowicz et al. [6] that indicate the presence of three peaks at  $1099$ ,  $803$  and  $464\text{ cm}^{-1}$ ; also, Yusof et al. [47] report vibrations in agreement with our data, located at  $1102$ ,  $804$  and  $470\text{ cm}^{-1}$ , respectively.

The chemical composition of RHA is reported in Table 1, resulting in a  $\text{SiO}_2$  content of 98.50 wt%.

**Table 1.** Percentage of chemical composition of RHA determined by XRF.

$\text{SiO}_2$	$\text{Al}_2\text{O}_3$	$\text{Fe}_2\text{O}_3$	$\text{CaO}$	$\text{Na}_2\text{O}$	$\text{MnO}$	$\text{TiO}_2$	$\text{MgO}$	$\text{P}_2\text{O}_5$
98.50	0.26	0.18	0.13	0.20	0.14	0.02	0.14	0.11

XRPD analysis reveals the absence of peaks in the spectrum of Experiment 1 in the time interval 2–8 h, thus resulting in amorphous composition (Figure 2a).

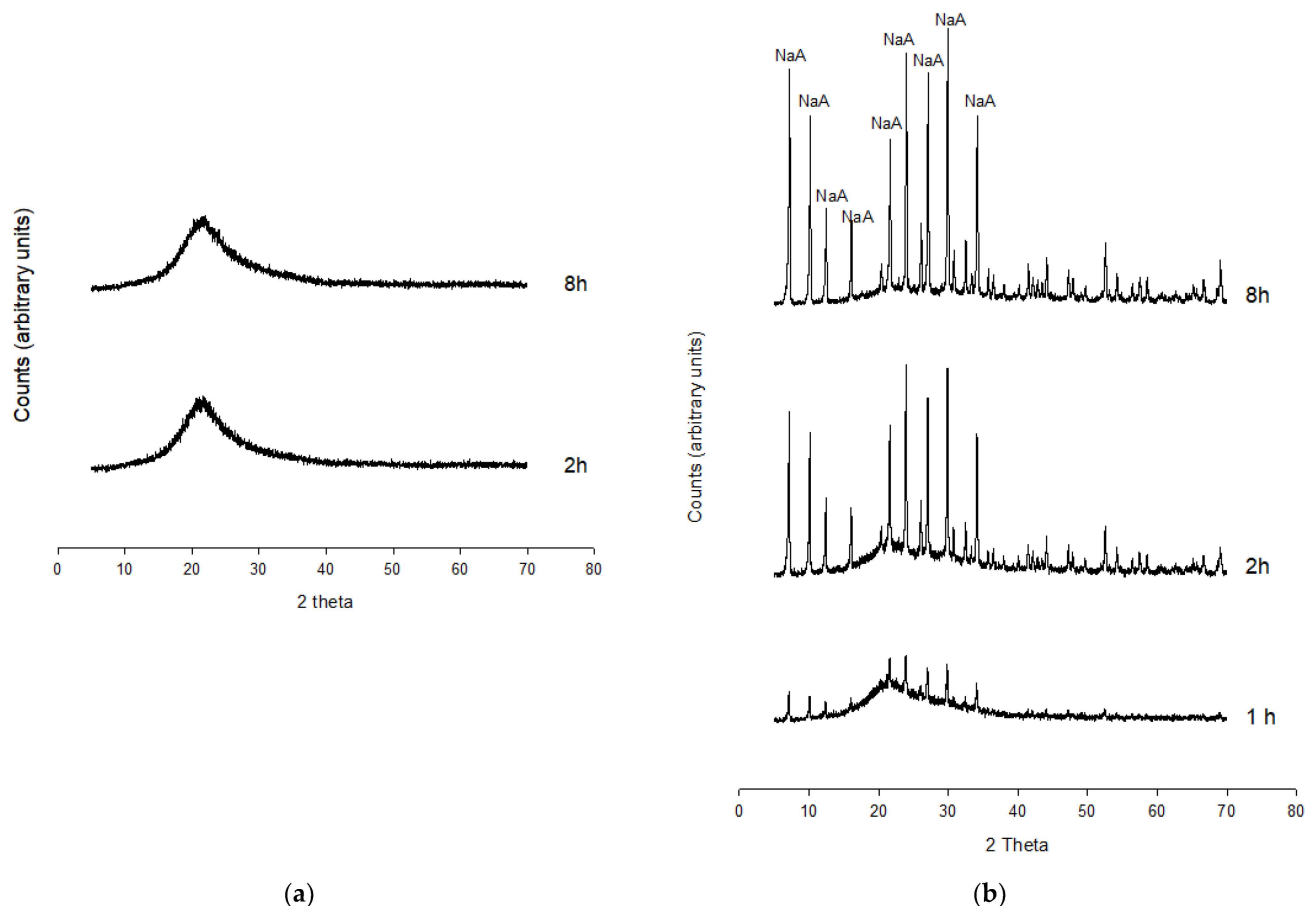


**Figure 2.** XRPD data. (a) XRPD pattern of Experiment 1, (b) XRPD pattern of Experiment 2.

The NaA zeolite is the main phase synthesized in Experiment 2 (Figure 2b). The first appearance is in fact attested at 1 h; the peak intensity increases over time, and the crystallization climax is reached after 8 h.

The beginning of the crystallization of the NaA zeolite is observed as an isolated phase at 2 h in Experiment 3 (Figure 3a); the intensity of the peaks increases after 4 h but the phase is no longer isolated, given the appearance of Analcime (ANA) at 4 h; then, NaA is associated with ANA and NaP in the time interval 6–8 h.

NaA crystallization starts as an isolated phase at 2 h in Experiment 4 (Figure 3b). The phase is associated with NaX at 4 h. Appearance of NaP is registered at 6 h, thus resulting in the overlapping of NaA, NaX and NaP. Disappearance of NaA is evidenced at 8 h, testifying to the progressive replacement of the NaA zeolite by the NaX and NaP.

All synthetic powders were analyzed by a Scanning Electron Microscope (SEM). Figure 4a,b report Scanning Electron Microscope (SEM) images of NaA crystals from Experiment 2 at 6 and 8 h, respectively. It results in a cubic morphology of the crystals and an average maximum length of crystals of around 3–4 microns.

Figure 5a,b report SEM images of crystals from Experiment 3. Figure 5a reports crystals of NaA at 4 h, while Figure 5b shows replacement of NaA by rounded euhedral crystals of ANA and acicular crystals of NaP at 8 h.

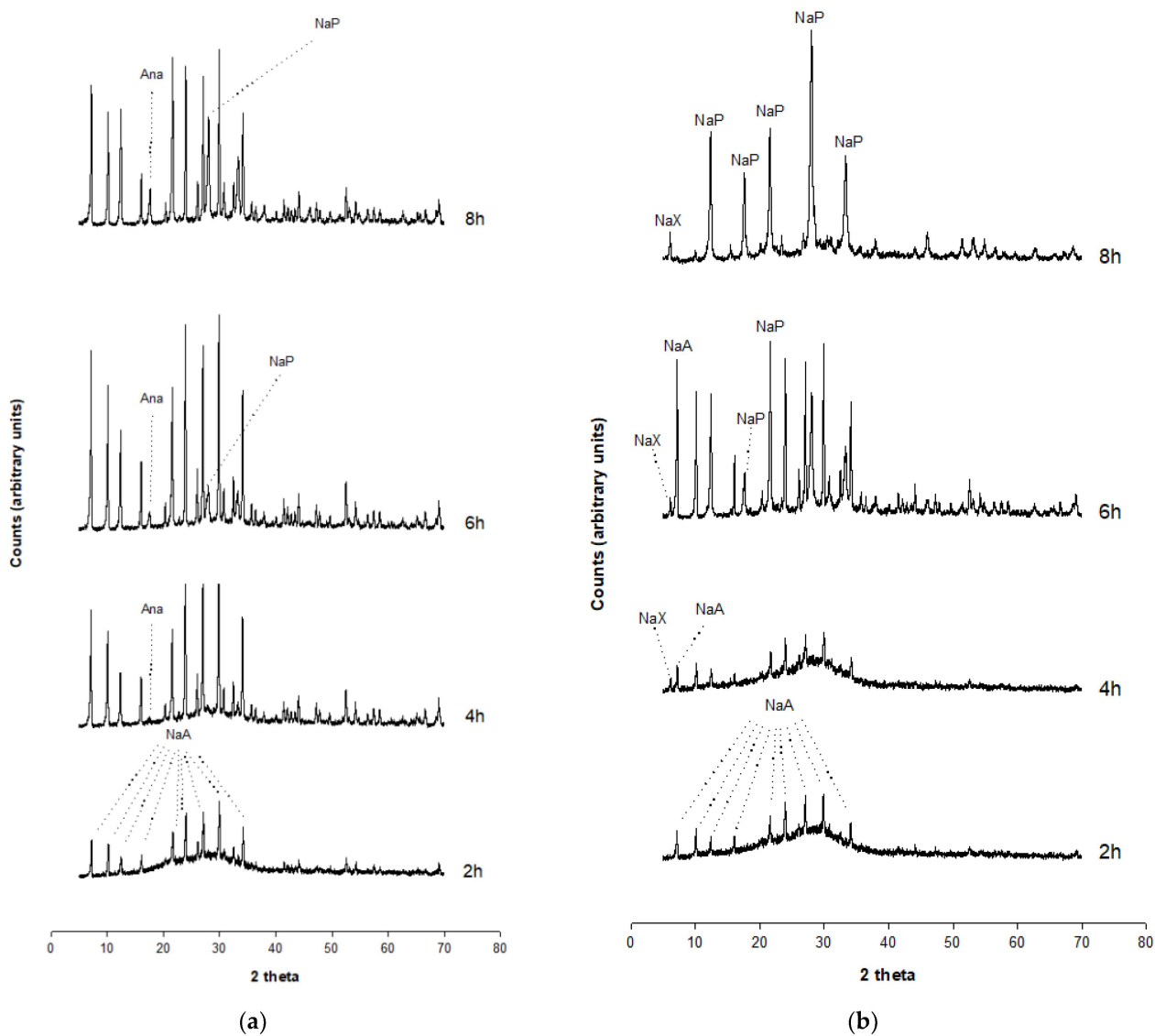


Figure 3. XRPD data. (a) XRPD pattern of Experiment 3, (b) XRD pattern of Experiment 4.

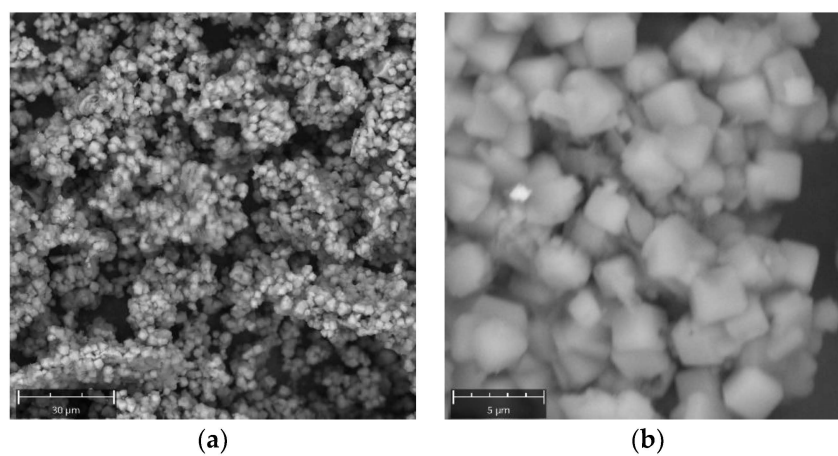
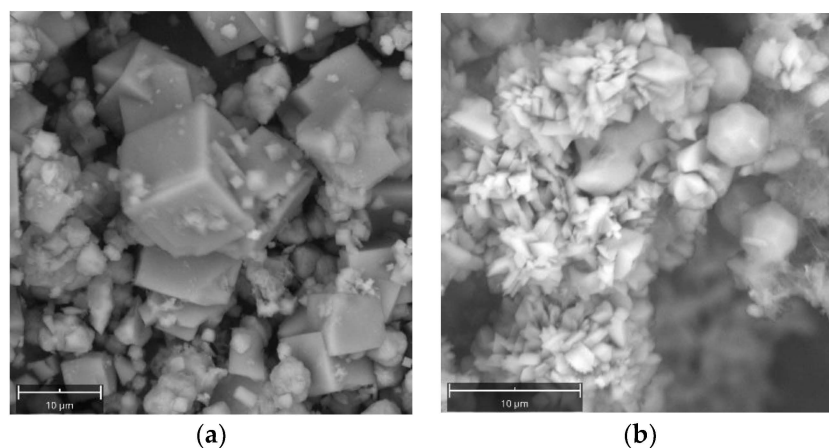
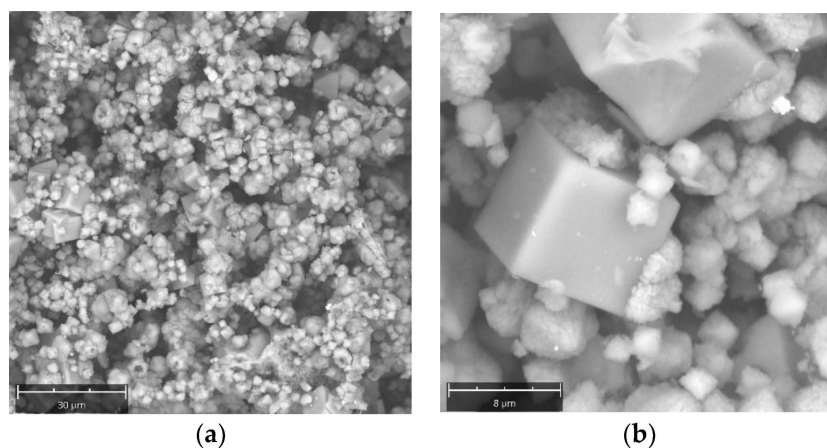


Figure 4. SEM images of NaA zeolite crystals for Experiment 2. (a) 6 h, (b) 8 h.



**Figure 5.** SEM images of zeolite crystals for Experiment 3. (a) 4 h, (b) 8 h.

Figure 6a,b report SEM images of crystals from Experiment 4. A mix of morphologies associated with different phases are observed, though their identification is difficult due to the low crystalline grain; it can be stated that it deals with NaX and NaP species, as determined by XRD analyses. Among these, characteristic NaA cubic crystals are evident, with an average size of 10 microns.



**Figure 6.** SEM images of zeolite crystals for Experiment 4. (a) 4 h, (b) 8 h.

The results of XRPD and SEM analyses indicate that Experiment 2 achieves the best result in obtaining the NaA zeolite as an isolated phase. Sixty degrees Celsius can be defined as the lowest temperature value at which the NaA zeolite crystallizes as an isolated phase, as achieved in Experiment 2. When the  $\text{SiO}_2/\text{Al}_2\text{O}_3$  ratio is increased to the value of 3.5 at the same temperature ( $60\text{ }^\circ\text{C}$ ) in Experiment 4, good results are not obtained, given the overlap of the phases.

The increase in the ratio  $\text{SiO}_2/\text{Al}_2\text{O}_3$  from 1.75 to 3.5 in fact makes the stability of the NaA zeolite unfavorable, delimiting its stability field at 6 h after the start of the synthesis run. The NaA zeolite is quickly consumed and replaced at 8 h by NaP and NaX, which are phases characterized by a higher structural silica content, just as observed by Breck [30].

For this reason, further characterizations were conducted on the sample at 8 h in Experiment 2.

The results of the quantitative phase analysis (QPA) are illustrated in Table 2. The cell parameters of NaA are refined with cubic symmetry, space group  $Fm-3c$ . The results of the Rietveld refinements provide cell values that are in good agreement with the structural model proposed by Gramlich and Meier [57]. It results in 93.5% of zeolitic phase achieved at 8 h.

**Table 2.** Results of the QPA analyses conducted on sample at 8 h in Experiment 2.

Sample + 10% Corundum Nist 676a	60 °C–8 h
$R_{wp}$	0.18
$R_p$	0.15
$CHI^2$	2.41
space group NaA	<i>Fm-3c</i>
$a$ (Å)	24.5932 (0.0035)
% amorphous	8.6 (14)
NaA	91.4 (18)

The observed and calculated profiles and difference plots for NaA and corundum NIST 676a are reported in Figure 7, showing very good agreement between the experimental data and the structural model used [57].

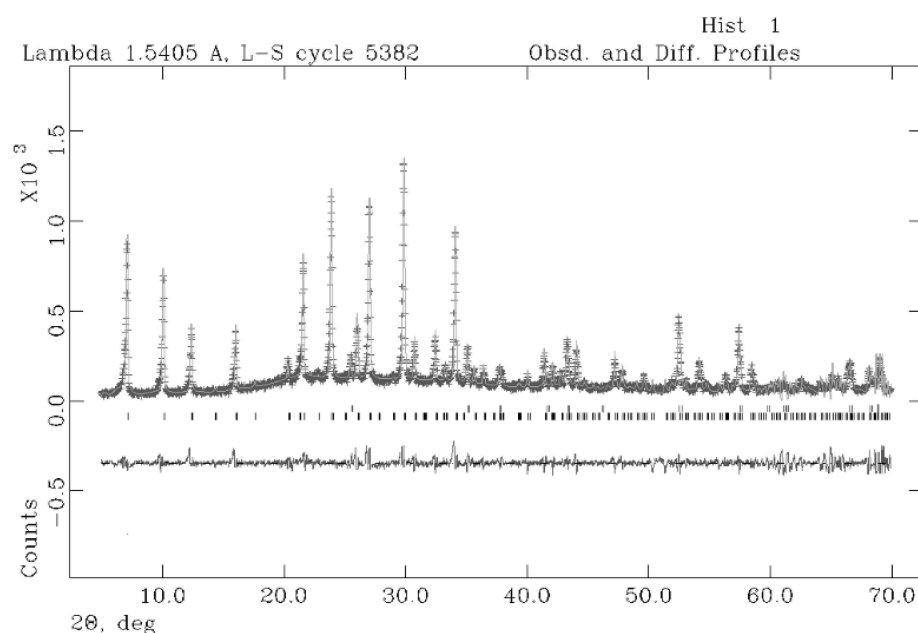


**Figure 7.** Rietveld refinement plot: observed (+) and calculated profiles and difference plot for NaA zeolite (8 h, Experiment 2) and corundum NIST 676a with tick marks at the position of the Bragg peaks. From the bottom: NaA zeolite, corundum NIST 676a.

Using the BET method, the obtained zeolite had a specific surface area of 6.10 m<sup>2</sup>/g, an average pore volume of 0.0029 cm<sup>3</sup> g<sup>−1</sup> and a pore size of 19.3959 Å. These values are relatively low, being coherent with data expected for this zeolite [6].

Figure 8 illustrates the results of the IR analysis. The main band is located at 968 cm<sup>−1</sup> and is related to the region of the asymmetric stretch. The value obtained is consistent with that known for the NaA zeolite [58], with reported values of 995 cm<sup>−1</sup> for the main band. In the 750–650 cm<sup>−1</sup> spectral zone, there is a band at 658 cm<sup>−1</sup> associated with the region of the symmetric stretch.

In the 650–500 cm<sup>−1</sup> spectral region, relative to the double-ring bond's vibration zone, there is a band at 541 cm<sup>−1</sup>. In the 500–420 cm<sup>−1</sup> sector, related to the deformation vibrations of the O-T-O bond, there is evidence of a band at 455 cm<sup>−1</sup>. The bands are in good agreement with those found by Flaningen et al. [58], Fotovat et al. [44] and Yusof et al. [47] for the NaA zeolite.

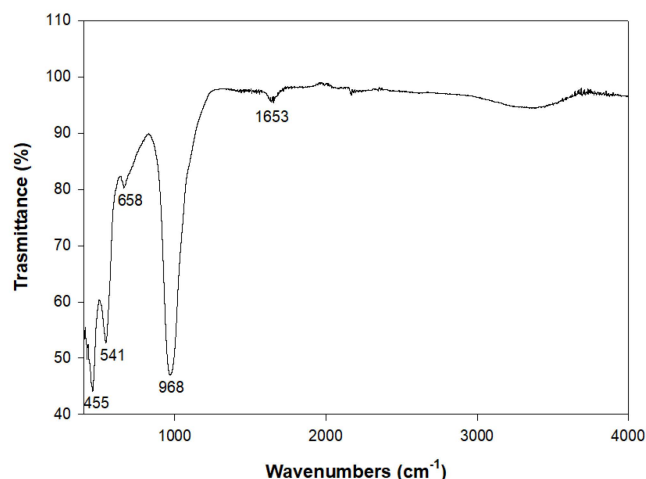


Figure 8. IR spectrum of the sample at 8 h—Experiment 2.

Figure 9 reports the Raman spectrum for the sample at 8 h of Experiment 2. The strongest band at  $486\text{ cm}^{-1}$  is related to the bending mode of four-membered Si-O-Al rings as reported by No et al. [59]. The bands at  $338$  and  $395\text{ cm}^{-1}$  are attributed to the bending mode of six-membered Si-O-Al rings as indicated by Dutta et al. [60]. The band at  $281\text{ cm}^{-1}$  is attributed to the bending mode of the eight-membered rings of the zeolite, just as observed by Yu et al. [61].

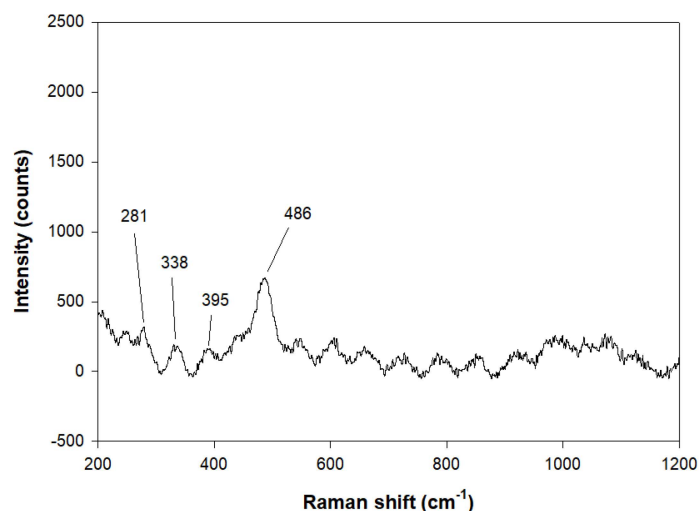


Figure 9. Raman spectra of the sample at 8 h—Experiment 2.

### 3. Materials and Methods

The RH sample coming from NE Spain was trituated, washed with water and dried at  $105\text{ }^{\circ}\text{C}$  for 24 h. Then, it was subjected to calcination with the following procedure: aliquots of RH were placed in open porcelain crucibles which were heated in a BE43N BICASA furnace (Bernareggio Italy), to the calcination temperature ( $550\text{ }^{\circ}\text{C}$ ). The heating rate of the sample was  $1.5\text{ }^{\circ}\text{C s}^{-1}$ . Once the calcination temperature was reached, the crucibles were left in the furnace for 5 h and then removed and cooled at room temperature. Following the calcination treatment, an RH ash (RHA) was obtained. The composition of RHA major elements was determined by X-ray fluorescence (XRF), by means of a Sequential X-ray WDXRF, Panalytical (Malvern, UK), Axios PW 4400/40 sequential spectrophotometer at Centres Científics i Tecnològics de la Universitat de Barcelona (CCiT-UB). The analysis strategy included the production of 3 fused pearls (original, duplicate and cleaning pearl in a Pt crucible and collector Pt dish, using LiI as a viscosity corrector) at a ratio dilution sample/lithium tetraborate 1/20. The high silica content of RHA represented a problem,



taking into account the range of composition of the international standards available for the calibration curve. This was overpassed with an ad hoc procedure consisting of mixing 1:2 and 1:3 proportions of international standards of basaltic composition (kindly provided to DG for Geological Survey of Japan) with the RHA, obtaining results in the calibration range rhyolite–andesite of the instrument. Since light elements, and especially Na, in low contents (i.e., lesser than 2.5% Na<sub>2</sub>O) [62] are a source of trouble, this was solved with an in-house calibration laboratory with internal standards also previously analyzed by AAS [63]. The spectrometer was calibrated using a set of more than 60 international standards [64,65].

The NaOH and NaAlO<sub>2</sub> used in the synthesis protocol were purchased from Riedel-de Haën (Honeywell Riedel-de Haën, Bucharest, Romania). The purity of the reagent was 99%. Zeolitic synthesis was operated under hydrothermal conditions and environment pressure by the mixing of silicatic and aluminatic solutions.

The silicatic solution was prepared with the following procedure: 0.95 g of the obtained RHA was dissolved in a 29cc NaOH 8 % solution (2M). The aluminatic solution was obtained as follows: 1.38 g NaAlO<sub>2</sub> was added to 29cc NaOH 8 % solution. The silicate solution was gradually mixed with aluminatic solution in the ratio of 1:1 for Experiments 1, 2 and 3 and 1:0,5 for Experiment 4. The initial mixtures had the following composition: 1.75 SiO<sub>2</sub>–1.00 Al<sub>2</sub>O<sub>3</sub>–5.46 Na<sub>2</sub>O–349 H<sub>2</sub>O (for Experiments 1, 2 and 3) and 3.50 SiO<sub>2</sub>–1.00 Al<sub>2</sub>O<sub>3</sub>–7.69 Na<sub>2</sub>O–536 H<sub>2</sub>O (for Experiment 4). The mixtures were homogenized for two hours with a magnetic stirrer.

Then, they were put inside stainless-steel hydrothermal reactors and heated at 40 °C–60 °C and 85 °C. In Table 3, the experimental conditions are reported, indicating the SiO<sub>2</sub>/Al<sub>2</sub>O<sub>3</sub>, Na<sub>2</sub>O/SiO<sub>2</sub> and H<sub>2</sub>O/Na<sub>2</sub>O ratios of the starting solutions and the temperatures of synthesis.

**Table 3.** Experimental conditions used in the four synthesis runs.

	SiO <sub>2</sub> /Al <sub>2</sub> O <sub>3</sub> Ratio	Na <sub>2</sub> O/SiO <sub>2</sub> Ratio	H <sub>2</sub> O/Na <sub>2</sub> O Ratio	T (°C)
1	1.75	3.1	63.9	40
2	1.75	3.1	63.9	60
3	1.75	3.1	63.9	85
4	3.50	2.19	69.7	85

Figure 10 shows the scheme of the experimental protocol.

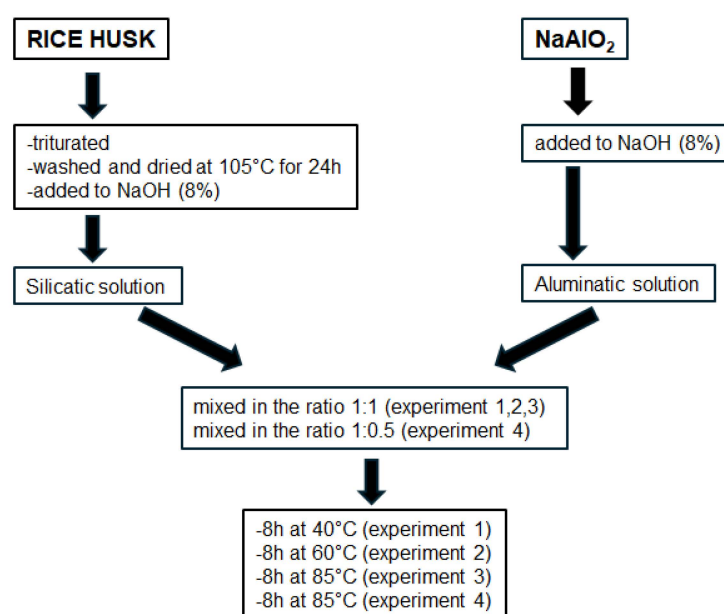


**Figure 10.** Scheme of experimental protocol.

The synthesis processes were proved by step-by-step XRD through periodic sampling. Samples obtained at different intervals were filtered from the solution, thoroughly washed with distilled water and oven dried at 40 °C for one day. Samples prepared as smears on glass slides were subjected to XRD analysis [35].

RHA and the products of synthesis were analyzed by powder X-ray diffraction (XRPD); the instrument was a RIGAKU (Osaka, Japan); “MiniFlex II” operating with a Bragg–Brentano geometry (CuK $\alpha$  = 1.518 Å, 30 kV, 15 mA, 5–70° 2 theta scanning interval, step size 0.02° 2 theta, data acquisition speed of 0.033°/s). Identification of zeolites and relative peak assignment were performed with reference to the following JCPDS code: 71-0962 for NaA, 00-019-1180 for ANA, 71-0962 for NaP and 63231-69-6 for NaX. Both the crystalline and amorphous phases in the synthesis powders were estimated using quantitative phase analysis (QPA) applying the combined Rietveld and reference intensity ratio (RIR) methods; corundum NIST 676a was added to each sample, amounting to 10% (according to the strategy proposed by Novembre et al. [66,67]) and the powder mixtures were homogenized by hand-grinding in an agate mortar. Data for the QPA refinement were collected in the angular range 5–70° 2 theta with steps of 0.02° and 10 s step<sup>-1</sup>, a divergence slit of 0.5° and a receiving slit of 0.1 mm.

Data were processed with the GSAS software 3.0 [68] and the graphical interface [69] starting with the structural models proposed by Gramlich and Meier [58] for NaA. The following parameters were refined: background parameters, zero shift, cell parameters and peak profiles [70–73].

Morphological analyses were obtained by means of scanning electron microscopy Phenom XL SEM–EDX (ThermoFisher Scientific, Dartford, UK); powders were analyzed according to the method explained in Novembre et al. [21] including dehydration of environmental moisture, mounting on auto adhesive stub, and metal coating. Due to the great capacity of water uptake of zeolites and the well-known disturbances in SEM observations, a double coating with graphite and vaporized Au was chosen. The instrumental operative conditions were as follows: high vacuum, accelerating voltage of 15 kV and 2–15  $\mu$ m beam diameter.

The specific surface and porosity were obtained by applying the BET (Brunauer–Emmett–Teller) method with N<sub>2</sub> using a Micromeritics (Norcross, GA, USA) ASAP2010 instrument (operating from 10 to 127 kPa).

IR spectra were obtained using a Shimadzu IRAffinity-1S FTIR spectrophotometer (Shimadzu Italia S.r.l., Milan, Italy) equipped with a sealed and desiccated interferometer, a DLATGS (Deuterated Triglycine Sulphate Doped with L-Alanine) detector and a single reflection diamond ATR crystal (QATR 10, Shimadzu Italia S.r.l., Milan, Italy). FTIR spectrum was recorded in the range from 4000 to 400 cm<sup>-1</sup> co-adding 45 interferograms at a resolution of 4 cm<sup>-1</sup> with Happ–Genzel apodization. The ATR crystal was carefully cleaned before each analysis, a background was recorded for each sample and the measurements were performed in triplicate [74].

Spectra manipulation was carried out with the software LabSolution IR version 2.27 (Shimadzu Italia S.r.l., Milan, Italy).

Raman spectrum of NaP-1 was obtained by confocal and high-performance Raman microscope XploRA PLUS (Horiba, Kyoto, Japan) with deep-cooled CCD detector technology. LabSpec 6.6.1.14 (Horiba, Japan) was employed to control, optimize and process the acquired data. Furthermore, data were processed through Origin 8.5 to optimize the results. Analysis was performed in the range of 50–1700 cm<sup>-1</sup> and with an 1800-line/mm grating.

#### 4. Conclusions

Silica extracted from rice husk, a highly available and economic agricultural waste, is used instead of pure chemicals in the synthesis of NaA zeolites.

Rice husk is calcined at 550 °C. Four sets of experiments were carried out at environmental pressure and hydrothermal conditions; the temperatures and SiO<sub>2</sub>/Al<sub>2</sub>O<sub>3</sub> ratio varied from 40° to 85 °C and 1.75 to 3.5, respectively.

No crystallization of zeolites was attested at 40 °C with a SiO<sub>2</sub>/Al<sub>2</sub>O<sub>3</sub> ratio of 1.75.

The optimal conditions for crystallization of Na-A zeolites were reached in Experiment 2, at 60° with a SiO<sub>2</sub>/Al<sub>2</sub>O<sub>3</sub> ratio of 1.75. Na-A growth was visible at 2 h and peak intensities increased, reaching the maximum values at 8 h.

The coeval presence of zeolitic phases (Na-A, NaP and ANA) was tested in Experiment 3 at 85 °C with a SiO<sub>2</sub>/Al<sub>2</sub>O<sub>3</sub> ratio of 1.75.

When increasing the SiO<sub>2</sub>/Al<sub>2</sub>O<sub>3</sub> ratio to 3.5 at 60 °C in Experiment 4, the Na-A stability field diminished and NaP and NaX formation was favored.

Good agreement with bibliographic data was obtained for the infrared and Raman behavior of the NaA zeolite synthesized in Experiment 2 at 8 h. When our experimental protocol is compared with the cited literature, a clear improvement is evident. The calcination temperature of rice husk was reduced from 700 °C to 550 °C, while the synthesis temperature was reduced from 100 °C to 60 °C. The effective assessment of the degree of success of the experiment is here defined for the first time from calculation by QPA of the percentage of crystallization vs. amorphous material and other impurities. The sample at 8 h of Experiment 2 reached 93.5%.

It must be said that if on the one hand a large amount of bibliography is available which testifies to numerous attempts to valorize the use of rice husk in the synthesis of NaA zeolites, on the other hand no work has been followed by an industrial transfer.

We believe that the results achieved with our work can be considered improvements compared to the past and are encouraging from the perspective of an industrial transfer of the experimental protocol. For the first time in this work, the synthesis of NaA zeolites is recorded at temperatures lower than 100 °C and with rice husk calcination temperatures of 550 °C. With reference to the characterization of the synthesis product, the degree of purity of the powders is defined here for the first time; the obtained value of 93.5% is crucial in defining the degree of success of the experimental protocol when considering that industry requires powders at a purity of at least 90%. We believe that the achievement of more advantageous synthesis conditions from an economic point of view and a precise characterization of the zeolite obtained represents a substantial turning point compared to the previous literature and paves the way for a future industrial transfer of the experimental protocol.

**Author Contributions:** Conceptualization, D.N. and D.G.; Data curation, D.N., D.G., L.M., A.C.T., G.R., M.C. and P.d.P.; Investigation, D.N., D.G., L.M., A.C.T., G.R., M.C. and P.d.P.; Methodology, D.N. and D.G.; Supervision, D.N. and D.G.; Writing—original draft, D.N.; Writing—review and editing, D.G., L.M., A.C.T., G.R., M.C. and P.d.P. All authors have read and agreed to the published version of the manuscript.

**Funding:** This research received no external funding.

**Institutional Review Board Statement:** Not applicable.

**Informed Consent Statement:** Not applicable.

**Data Availability Statement:** The original contributions presented in the study are included in the article, further inquiries can be directed to the corresponding author.

**Acknowledgments:** The authors greatly acknowledge the technical staff at Universitat of Barcelona (CCiT-UB) and Chieti for their help during the development of the work. M.Menéndez (Biology fac., UB) helped us with the calcination of RH.

**Conflicts of Interest:** The authors declare no conflicts of interest.

## References

1. Mehta, P.K. Rice Husk Ash—A Unique Supplementary Cementing Material. *Adv. Concr. Technol.* **1992**, *2*, 407–431.
2. Maiti, S.; Dey, S.; Purakayastha, S.; Ghosh, B. Physical and thermochemical characterization of rice husk char as a potential biomass energy source. *Bioresour. Technol.* **2006**, *97*, 2065–2070. [[CrossRef](#)] [[PubMed](#)]
3. Hyun, T.J.; Yoon, K.P.; Young, S.K.; Ji, Y.L.; Bhagiyalakshmi, M. Highly siliceous MCM-48 from rice husk ash for CO<sub>2</sub> adsorption. *Int. J. Greenh. Gas Con.* **2009**, *3*, 545–549.

4. Bhavornthanayod, C.; Rungrojchaipon, P. Synthesis of zeolite A membrane from rice husk ash. *J. Met. Mater. Miner.* **2009**, *19*, 79–83.
5. Mohamed, R.M.; Mkhallid, I.A.; Barakat, M.A. Rice husk ash as a renewable source for the production of zeolite NaY and its characterization. *Arab. J. Chem.* **2015**, *8*, 48–53. [[CrossRef](#)]
6. Petkowicz, D.I.; Rigo, R.T.; Radtke, C.; Pergher, S.B.; dos Santos, J.H.Z. Zeolite NaA from Brazilian Chrysotile and rice husk. *Micropor. Mesopor. Mat.* **2008**, *116*, 548–554. [[CrossRef](#)]
7. Arcos, C.A.; Macías Pintob, D.; and Rodríguez Páez, J.E. La cascarilla de arroz como fuente de SiO<sub>2</sub> Husk of rice as source of SiO<sub>2</sub>. *Rev. Fac. Ing. Univ. Antioquia.* **2007**, *41*, 7–20.
8. Barthey, B.R.; Gretella, M.C. Solar grade silicon. *J. Mater. Sci.* **1982**, *17*, 3077–3096. [[CrossRef](#)]
9. Johar, N.; Ahmad, I.; Dufresne, A. Extraction, Preparation and Characterization of Cellulose Fibres and Nanocrystals from Rice Husk. *Ind. Crops Prod.* **2012**, *37*, 93–99. [[CrossRef](#)]
10. Dalai, A.K.; Rao, M.S. Synthesis of NaX Zeolite Using Silica from Rice Husk Ash. *Ind. Eng. Chem. Prod. Res. Dev.* **1985**, *24*, 465–468. [[CrossRef](#)]
11. Gookhale, K.V.G.K.; Dalai, A.K.; Rao, M.S. Thermal characteristics of synthetic sodium zeolites prepared with silica from rice-husk ash. *J. Therm. Anal.* **1986**, *31*, 33–39. [[CrossRef](#)]
12. Kongkachuichay, P.; Lohsoontorn, P. Phase diagram of zeolite synthesized from perlite and rice husk ash. *ScienceAsia* **2006**, *32*, 13–16. [[CrossRef](#)]
13. Wittayakun, J.; Khemthong, P.; Prayoonkarach, S. Synthesis and characterization of zeolite NaY from rice husk silica. *Korean J. Chem. Eng.* **2008**, *25*, 861–864. [[CrossRef](#)]
14. Khabuanchalead, S.; Khemthong, P.; Prayoonpokarack, S.; Wittayakun, J. Transformation of zeolite NaY synthesized from rice husk silica to NaP during hydrothermal synthesis. *J. Sci. Technol.* **2008**, *15*, 225–231.
15. Rahman, M.M.; Hasnidab, N.; Wan Nik, W.B. Preparation of Zeolite Y Using Local Raw Material Rice Husk as a Silica Source. *J. Sci. Res.* **2009**, *1*, 285–291. [[CrossRef](#)]
16. Klunk, M.A.; Das, M.; Dasgupta, S.; Impiombato, A.N.; Caetano, N.R.; Wander, P.R.; Mendes Moraes, C.A. Comparative study using different external sources of aluminum on the zeolites synthesis from rice husk ash. *Mater. Res. Express* **2020**, *7*, 015023. [[CrossRef](#)]
17. Solihat, I.; Sulistiawaty, L.; Syaifie, P.H.; Taufiq, A. Removal of Cu Metals from Wastewater by Adsorption using Synthetic Zeolites from Rice Husk and Corn cob. *Molekul* **2020**, *15*, 105–113. [[CrossRef](#)]
18. Alosaimi, E.H.; Alsohaimi, I.H.; Dahan, T.E.; Chen, Q.; Younes, A.A.; El-Gammal, B.; Melhi, S. Photocatalytic Degradation of Methylene Blue and Antibacterial Activity of Mesoporous TiO<sub>2</sub>-SBA-15 Nanocomposite Based on Rice Husk. *Adsorpt. Sci. Technol.* **2021**, *2021*, 9290644. [[CrossRef](#)]
19. Ji, F.; Zhang, C.; Mi, Y. Study on the effect of inorganic aluminum sources on ZSM-5 zeolite synthesis by solvent-free method from rice husk ash. *Chem. Pap.* **2024**, *78*, 1217–1226. [[CrossRef](#)]
20. Sherry, H.S. Ion-exchange properties of the natural zeolite erionite. *Clay. Clay Miner.* **1979**, *27*, 231–237. [[CrossRef](#)]
21. Novembre, D.; Di Sabatino, B.; Gimeno, D.; Garcia Valles, M.; Martinez-Manent, S. Synthesis of Na-X zeolites from tripolaceous deposits (Crotone, Italy) and volcanic zeolitized rocks (Vico Volcano, Italy). *Micropor. Mesopor. Mat.* **2004**, *75*, 1–11. [[CrossRef](#)]
22. The Database of Zeolite Structures 1996–2016, The IZA-SC. 2016. Available online: <https://www.iza-structure.org/databases/> (accessed on 1 July 2024).
23. Collins, F.; Rozhkovskayaa, A.; Outramb, J.G.; Millar, J. A critical review of waste resources, synthesis, and applications for Zeolite LTA. *Microp. Mesop. Mat.* **2020**, *291*, 109667. [[CrossRef](#)]
24. Cardoso, A.C.; Duchemin, J.; Magoarou, P.; Premazzi, G. Criteria for the identification of freshwaters subject to eutrophication. Their use for the implementation of the ‘Nitrates’ and Urban Waste Treatment directives. *Eur. Comm. Environ. Qual. Life Ser.* **2001**, *19810*, 90.
25. Ghoufi, A.; Gaberova, L.; Rouquerol, J.; Vincent, D.; Llewellyn, P.L.; Maurin, G. Adsorption of CO<sub>2</sub>, CH<sub>4</sub> and their binary mixture in Faujasite NaY: A combination of molecular simulations with gravimetry–manometry and microcalorimetry measurements. *Microporous Mesoporous Mater.* **2009**, *119*, 117–128. [[CrossRef](#)]
26. Montanari, T.; Busca, G. On the mechanism of adsorption and separation of CO<sub>2</sub> on LTA zeolites: An IR investigation. *Vib. Spectrosc.* **2008**, *46*, 45–51. [[CrossRef](#)]
27. Sharma, V.K.; Gautam, S.; Mitra, S.; Mukhopadhyay, R. Dynamics of propylene adsorbed in Na–Y and Na–ZSM5 zeolites: A QENS and MD simulation study. *Z. Phys. Chem.* **2010**, *224*, 133–152. [[CrossRef](#)]
28. Bernier-Oviedo, D.J.; Rincón-Moreno, J.A.; Solanilla-Duqué, J.F.; MuñozHernández, J.A.; Váquiro-Herrera, H.A. Comparison of two pretreatments methods to produce second-generation bioethanol resulting from sugarcane bagasse. *Ind. Crops Prod.* **2018**, *122*, 414–421. [[CrossRef](#)]
29. Cowan, M.M.; Abshire, K.Z.; Houk, S.L.; Evans, S.M. Antimicrobial efficacy of a silver-zeolite matrix coating on stainless steel. *J. Ind. Microbiol. Biotechnol.* **2003**, *30*, 102–106. [[CrossRef](#)]
30. Breck, D. Zeolite Molecular Sieves. John Wiley & Sons: New York, NY, USA, 1984; 771p.
31. Coombs, D.S.; Ellis, A.J.; Fyfe, W.S.; Taylor, A.M. The zeolite facies, with comments on the interpretation of hydrothermal syntheses. *Geochim. Cosmochim. Acta* **1959**, *17*, 53–107. [[CrossRef](#)]

32. Novembre, D.; Di Sabatino, B.; Gimeno, D.; Pace, C. Synthesis and characterization of Na-X, Na-A and Na-P zeolites and hydroxysodalite from metakaolinite. *Clay Miner.* **2011**, *46*, 336–354. [[CrossRef](#)]
33. Novembre, D.; Gimeno, D.; Del Vecchio, A. Improvement in the synthesis conditions and studying the physicochemical properties of the zeolite Li-A(BW) obtained from a kaolinitic rock. *Sci. Rep.* **2020**, *10*, 5715–5723. [[CrossRef](#)]
34. Novembre, D.; Gimeno, D. Synthesis and characterization of analcime (ANA) zeolite using a kaolinitic rock. *Sci. Rep.* **2021**, *11*, 13373–13382. [[CrossRef](#)] [[PubMed](#)]
35. Novembre, D.; Gimeno, D.; Del Vecchio, A. Synthesis and characterization of Na-P<sub>1</sub> (GIS) zeolite using a kaolinitic rock. *Sci. Rep.* **2021**, *11*, 4872–4883. [[CrossRef](#)] [[PubMed](#)]
36. De Lucas, A.; Uguina, M.A.; Covian, I.; Rodriguez, L. Synthesis of 13X zeolite from calcined kaolin 352 D. Novembre et al. and sodium silicates for use in detergents. *Ind. Eng. Chem. Res.* **1992**, *31*, 2134–2140. [[CrossRef](#)]
37. Covian, I. Sintesis de Zeolite 13X para su Uso en Detergentes. Ph.D. Thesis, Universidad Complutense de Madrid, Madrid, Spain, 1991.
38. Abdmeziem-Hamoudi, K.; Siffert, B. Synthesis of molecular sieve zeolites from a smectite- type clay material. *App. Clay Sci.* **1989**, *4*, 1–9. [[CrossRef](#)]
39. Lee, M.J.; Cho, J.; Huh, H.; Choi, B. Studies on synthesis of X-type zeolite from the natural mordenite. *J. Korean Ceram. Soc.* **1994**, *31*, 1570–1576.
40. Gualtieri, A.F. Synthesis of sodium zeolites from a natural halloysite. *Phys. Chem. Miner.* **2001**, *28*, 719–728. [[CrossRef](#)]
41. Novembre, D.; Di Sabatino, B.; Gimeno, D. Synthesis of Na-A zeolite from 10 Å halloysite and a new crystallization kinetic model for the transformation of Na-A into HS zeolite. *Clay. Clay Miner.* **2005**, *53*, 28–36. [[CrossRef](#)]
42. Boukadir, D.; Bettahar, N.; Derriche, Z. Etude de la synthese des zeolites 4A et HS a partir de produits naturels. *Ann. Chim. Sci. Mat.* **2002**, *27*, 1–13. [[CrossRef](#)]
43. Tanaka, H.; Sakai, Y.; Hino, R. Formation of Na-A and Na-X zeolites from waste solutions in conversion of coal fly ash to zeolites. *Mater. Res. Bull.* **2002**, *37*, 1873–1884. [[CrossRef](#)]
44. Fotovat, F.; Kazemian, H.; Kazemini, M. Synthesis of Na-A and faujasitic zeolites from high silicon fly ash. *Mater. Res. Bull.* **2009**, *44*, 913–917. [[CrossRef](#)]
45. Maia, A.A.B.; Angélica, R.S.; Neves, R.F. Use of industrial kaolin waste from the Brazilian Amazon region for synthesis of zeolite A. *Clay Miner.* **2011**, *46*, 127–136. [[CrossRef](#)]
46. Nur, H. Direct synthesis of NaA zeolite from rice husk and carbonaceous rice husk ash. *Indones. J. Agric. Sci.* **2001**, *1*, 40–45.
47. Yusof, A.M.; Malek, N.A.N.N.; Rashid, N.A.A. Hydrothermal conversion of rice husk ash to faujasite-types and NaA-type of zeolites. *J. Porous. Mater.* **2010**, *17*, 39–47. [[CrossRef](#)]
48. Azizi, S.N.; Maryam, Y. Synthesis of Zeolites NaA and Analcime Using Rice Husk Ash as Silica Source without Using Organic Template. *J. Mat. Sci.* **2010**, *45*, 5692–5697. [[CrossRef](#)]
49. Tan, W.C.; Yap, S.Y.; Matsumoto, A.; Othman, R.; Yeoh, F.Y. Synthesis and characterization of zeolites NaA and NaY from rice husk ash. *Adsorption* **2011**, *17*, 863–868. [[CrossRef](#)]
50. Ghasemi, Z.; Younesi, H. Preparation and characterization of nanozeolite NaA from rice husk at room temperature without organic additives. *J. Nanomater.* **2011**, *2011*, 858961. [[CrossRef](#)]
51. Ghasemi, Z.; Younesi, H. Preparation of Free-Template Nanometer-Sized Na-A and -X Zeolites From Rice Husk Ash. *Waste Biomass Valor.* **2012**, *3*, 61–74. [[CrossRef](#)]
52. Tepamat, T.; Mongkolkachit, C.; Wasanapiarnpong, T. Synthesis of zeolite NaA and activated carbon composite from rice husk. *Suranaree J. Sci. Technol.* **2014**, *21*, 119–123.
53. Ahmedzeki, N.S.; Abbas, M.N.; Joodee, A.M.; Jaed, Y.M. Waste resources utilization for zeolite a synthesis. *J. Chem. Technol. Metall.* **2018**, *53*, 239–244.
54. Wang, Y.; Du, T.; Jia, H.; Qiu, Z.; Song, Y. Synthesis, characterization and CO<sub>2</sub> adsorption of NaA, NaX and NaZSM-5 from rice husk ash. *Solid State Sci.* **2018**, *86*, 24–33. [[CrossRef](#)]
55. Madhu, J.; Santhanam, A.; Natarajan, M.; Velauthapillai, D. CO<sub>2</sub> adsorption performance of template free zeolite A and X synthesized from rice husk ash as silicon source. *RSC Adv.* **2022**, *12*, 23221. [[CrossRef](#)] [[PubMed](#)]
56. Treacy, M.M.J.; Higgins, J.B. Linde type A, hydrated. In *Collection of Simulated XRD Power Patterns for Zeolites*, 5th ed.; Elsevier: Amsterdam, The Netherlands, 2007; pp. 252–253.
57. Gramlich, V.; Meier, W.M. The crystal structure of hydrated NaA: A detailed refinement of a pseudosymmetric zeolite structure. *Z. Kristallogr.* **1971**, *133*, 134–149. [[CrossRef](#)]
58. Flanigen, E.M.; Khatami, H.; Szymanski, H.A. Infrared Structural Studies of Zeolite Frameworks. In *Molecular Sieve Zeolites, Advances in Chemistry 101*; Flanigen, E.M., Sand, L.B., Eds.; American Chemical Society: Washington DC, USA, 1971; pp. 201–229.
59. No, K.T.; Bae, D.H.; Jhon, M.S. Lattice vibrational calculation of A-type zeolite using the pseudolattice method. *J. Phys. Chem.* **1986**, *90*, 1772. [[CrossRef](#)]
60. Dutta, P.K.; Shieh, D.C.; Puri, M. Raman Spectroscopic Study of the Synthesis of Zeolite YJ. *J. Phys. Chem.* **1987**, *91*, 2332–2336. [[CrossRef](#)]
61. Yu, Y.; Xiong, G.; Li, C.; Xiao, F.S. Characterization of aluminosilicate zeolites by UV Raman spectroscopy. *Microp. Mesopor. Mat.* **2008**, *46*, 23–34. [[CrossRef](#)]

62. Gimeno, D.; Puges, M. Caracterización química de la vidriera histórica de Sant Pere i Sant Jaume (Monestir de Pedralbes, Barcelona). *Bol. Soc. Esp. Ceram. Vidr.* **2002**, *41*, 13–20. [[CrossRef](#)]
63. Aulinas, M.; Gimeno, D.; Fernandez-Turiel, J.L.; Perez-Torrado, F.J.; Rodriguez-Gonzalez, A.; Gasperini, D. The Plio-Quaternary magmatic feeding system beneath Gran Canaria (Canary Islands, Spain): Constraints from thermobarometric studies. *J. Geol. Soc.* **2010**, *167*, 785–801. [[CrossRef](#)]
64. Aulinas, M.; Civetta, L.; Di Vito, M.; Orsi, G.; Gimeno, D.; Fernandez Turiel, J.L. The Plinian Mercato eruption of Somma Vesuvius: Magma chamber processes and eruption dynamics. *Bull. Volcanol.* **2008**, *70*, 825–840. [[CrossRef](#)]
65. Gisbert, G.; Gimeno, D. Ignimbrite correlation using whole-rock geochemistry: An example from the Sulcis (SW Sardinia, Italy). *Geol. Mag.* **2017**, *154*, 740–756. [[CrossRef](#)]
66. Novembre, D.; Gimeno, D.; d’Alessandro, N.; Tonucci, L. Hydrothermal synthesis and characterization of kalsilite by using a kaolinitic rock from Sardinia, Italy, and its application in the production of biodiesel. *Mineral. Mag.* **2018**, *82*, 961–973. [[CrossRef](#)]
67. Novembre, D.; Pace, C.; Gimeno, D. Synthesis and characterization of wollastonite-2M by using a diatomite precursor. *Miner. Mag.* **2018**, *82*, 95–110. [[CrossRef](#)]
68. Larson, A.C.; Von Dreele, R.B. GSAS: General Structure Analysis System. Document Laur 86-748. *Los Alamos Natl. Lab* **1997**, 121–124.
69. Toby, B.H. EXPGUI, a Graphical User Interface for GSAS. *J. Appl. Crystallogr.* **2001**, *34*, 210–213. [[CrossRef](#)]
70. Novembre, D.; Gimeno, D. The solid-state conversion of kaolin to KAlSiO<sub>4</sub> minerals: The effects of time and temperature. *Clays Clay Miner.* **2017**, *65*, 355–366. [[CrossRef](#)]
71. Novembre, D.; Gimeno, D.; Poe, B. Synthesis and Characterization of Leucite Using a Diatomite Precursor. *Sci. Rep.* **2019**, *9*, 10051–10061. [[CrossRef](#)]
72. Novembre, D.; Pace, C.; Gimeno, D. Syntheses and characterization of zeolites K-F and W type using a diatomite precursor. *Mineral. Mag.* **2014**, *78*, 1209–1225. [[CrossRef](#)]
73. Novembre, D.; Gimeno, D.; Cappelletti, P.; Graziano, S.F. A case study of zeolitization process: “tufo Rosso a Scorie Nere” (Vico Volcano, Italy): Inferences for a general model. *Eur. J. Mineral.* **2021**, *33*, 315–328. [[CrossRef](#)]
74. Ciulla, M.; Canale, V.; Wolicki, R.D.; Pilato, S.; Bruni, P.; Ferrari, S.; Siani, G.; Fontana, A.; Di Profio, P. Enhanced CO<sub>2</sub> Capture by Sorption on Electrospun Poly (Methyl Methacrylate). *Separations* **2023**, *10*, 505–521. [[CrossRef](#)]

**Disclaimer/Publisher’s Note:** The statements, opinions and data contained in all publications are solely those of the individual author(s) and contributor(s) and not of MDPI and/or the editor(s). MDPI and/or the editor(s) disclaim responsibility for any injury to people or property resulting from any ideas, methods, instructions or products referred to in the content.